Polymer Journal (2019) 51:91–96
https://doi.org/10.1038/s41428-018-0116-9

ORIGINAL ARTICLE

Hole-transporting diketopyrrolopyrrole-thiophene polymers and their additive-free application for a perovskite-type solar cell with an efficiency of 16.3%

Hirofumi Maruo[1] · Yusuke Sasaki[1] · Kohei Harada[1] · Koki Suwa[1] · Kenichi Oyaizu[1] · Hiroshi Segawa[2] · Kenneth Carter[3] · Hiroyuki Nishide[1]

Received: 13 June 2018 / Revised: 29 July 2018 / Accepted: 2 August 2018 / Published online: 23 August 2018

Abstract

Conjugated polymers of diketopyrrolopyrrole (DPP) and thiophene, especially 2,5-di-2-thienyl-thieno[3,2-*b*]thiophene, were characterized based on their molecular packing orientation, and they showed a π–π stacking distance of 3.6 Å and a high field-effect hole mobility on the order of 10^{-2} cm^2/Vs. Perovskite solar cells fabricated with the genuine or both oxidant- and salt dopant-free polymer as the hole-transporting layer displayed high photoconversion efficiencies of 16.3% as well as high durability.

Introduction

Hole-transporting organic polymers with a planar π-conjugated structure have been extensively studied for their potential applications as hole-transporting layers in electronic and photoelectronic devices [1–7]. Among the π-conjugated units of these polymers, diketopyrrolopyrrole (DPP) is of great interest because of its exceptionally high carrier-transport capability as well as its high thermal and photostability. These characteristics are derived from the doubly β-fused pyrrole, which alleviates steric repulsion to maintain a highly coplanar structure and efficient π-delocalization [8–10]. Two α-halogen substituted DPPs were polymerized through facile coupling reactions [11–13]. DPP polymers condensed from thiophenes, especially fused thiophenes, e.g., thienothiophene, showed extended π-conjugated and longer planar structures [14, 15], which often possessed strong π–π intermolecular interactions between the electron-donating thiophene and the electron-accepting DPP moieties, leading to morphologically well-ordered semicrystalline structures and an extremely high hole mobility (12 cm^2/Vs) comparable to that (14 cm^2/Vs) [16–22] of thienoisoindigo-naphthalene polymer. The molecular orientation strongly affects the hole mobility of conjugated polymers: two- or three-dimensional structures allow anisotropic carrier transport, and the symmetric nature of the DPP units favors an alignment oriented along the polymer chains. The excellent carrier-transport properties with a wide range of photoabsorption wavelengths allow the utilization of this material for the photoabsorption layers of organic bulk-heterojunction photovoltaic cells [23–25].

Perovskite solar cells using methylammonium lead halide ($CH_3NH_3PbI_3$) as the photoabsorption layer are emerging as a new class of photovoltaic cells [26–31]. The reported photoconversion efficiencies have increased dramatically in the past few years, and several groups have achieved efficiencies greater than 20% [32–34]. The hole-transporting material plays an important role in the solar cell in promoting hole extraction as well as in preventing internal charge recombination [35]. 2,2′,7,7′-Tetrakis

Electronic supplementary material The online version of this article (https://doi.org/10.1038/s41428-018-0116-9) contains supplementary material, which is available to authorized users.

✉ Hiroyuki Nishide
nishide@waseda.jp

[1] Department of Applied Chemistry and Research Institute for Science and Engineering, Waseda University, Tokyo 169-8555, Japan

[2] Research Center for Advanced Science and Technology, The University of Tokyo, Tokyo 153-8904, Japan

[3] Department of Polymer Science and Engineering, University of Massachusetts–Amherst, Amherst, MA 01003, USA

(*N,N′*-di-*p*-methoxyphenylamine)-9,9′-spirobifluorene (spiro-OMeTAD) is often used due to its excellent photovoltaic performance [26]. However, other hole transporting materials are desirable because the charge-carrier mobility of spiro-OMeTAD remains relatively low and its durability is limited due to the bridged structure and side reactions caused by the addition of oxidizing dopants such as tris(2-(1H-pyrazol-1-yl)-4-tert-butylpyridine)cobalt (III) tri[bis (trifluoromethane)sulfonimide]. Poly[bis(4-phenyl)(2,4,6-trimethylphenyl)amine] (often abbreviated PTAA), a representative commercially available arylamine polymer, is also often used as the hole-transporting polymer; cells fabricated with the polymer yielded high conversion efficiencies because of its adequate energy level and ability to form thin layers [36]. However, a multistep synthesis procedure is necessary, and a lithium salt was added as a dopant to generate the hole-transport ability, which would also limit the durability of the cells. Conjugated polymers with a high hole mobility without the addition of a dopant are desirable for preparing a hole-transporting material with high photovoltaic performance for perovskite solar cells. Although DPP polymers have been applied in solar cells, their photoconversion efficiencies remain low [37, 38].

This paper described a series of DPP-thiophene polymers, such as poly[[2,5-bis(2-hexyldecyl)-2,3,5,6-tetrahydro-3,6-dioxopyrrolo[3,4-*c*]pyrrole-1,4-diyl]-*alt*-[2,5-di(2-thienyl)thieno[3,2-*b*]thiophene]], which resulted in a closely packed lamellar structure and a very large field-effect hole mobility. The genuine polymers were applied as the hole-transporting material for perovskite-type solar cells, which performed with a high fill factor of 0.75 and a photoconversion efficiency of 16.3%. The durability of the hole-transporting layer in the absence of either an oxidizing agent or a salt additive was also demonstrated.

Experimental section

Materials

Polymers **1**–**4** were synthesized according to literature methods [34, 35] by modifying the reaction conditions: **1** was synthesized via a Yamamoto coupling, **2** and **4** were prepared via a Stille coupling, and **3** was prepared via a Suzuki coupling; poly[[2,5-bis(2-hexyldecyl)-2,3,5,6-tetrahydro-3,6-dioxopyrrolo[3,4-*c*]pyrrole-1,4-diyl]-*alt*-(2,2′-bis-thiophene)-5,5′-diyl]]) (**1**), poly[[2,5-bis(2-hexyldecyl)-2,3,5,6-tetrahydro-3,6-dioxopyrrolo[3,4-*c*]pyrrole-1,4-diyl]-*alt*-(2,2′,5′,2″-terthiophene)-5,5′-diyl]]) (**2**), poly[[2,5-bis(2-hexyldecyl)-2,3,5,6-tetrahydro-3,6-dioxopyrrolo[3,4-*c*]pyrrole-1,4-diyl]-*alt*-((2,2′,5′,2″,5″,2‴-tetrathiophen))-5,5′-diyl]]) (**3**), and poly[[2,5-bis(2-hexyldecyl)-2,3,5,6-tetrahydro-3,6-dioxopyrrolo[3,4-*c*]pyrrole-1,4-diyl]-*alt*-((2,5-di(2-thienyl)thieno[3,2-*b*]thiophene))] (**4**).

For **1**, 3,6-bis(5-bromo-2-thienyl)-2,5-bis(2-hexyldecyl)-2,5-dihydro-pyrrolo[3,4-c]pyrrole-1,4-dione (1.82 g), 2,2′-dipyridyl (385 mg), bis(cyclooctadiene)nickel (0) ($Ni(COD)_2$, 660 mg) and anhydrous THF (75 mL) were added to a dry 200 mL flask. The mixture was heated to 60 °C for 3 h after stirring at room temperature for 1.5 h and finally refluxed for 2 h. The mixture formed a precipitate upon addition of methanol, and the dark green precipitate was isolated by filtration. The precipitate was Soxhlet extracted with methanol, acetone, and hexane. The final fraction was reprecipitated from its THF solution with methanol and vacuum dried to afford a dark blue polymer (245 mg, 17%). ^{1}H NMR ($CDCl_3$, 500 MHz) δ (p.p.m.) 9.24–8.92 (*b*, 4 H), 7.09 (*b*, 4 H), 4.03 (*b*, 4 H), 1.93 (*b*, 2 H), 1.33–1.17 (*b*, 48 H), 0.91–0.76 (*b*, 12 H). GPC: M_n = 12,000; PDI = 2.0.

For **2**, 3,6-bis(5-bromo-2-thienyl)-2,5-bis(2-hexyldecyl) 2,5-dihydro-pyrrolo[3,4-*c*]pyrrole-1,4-dione (970 mg), 2,5-bis(trimethylstannyl)thiophene (440 mg), and $Pd(PPh_3)_2Cl_2$ (22.5 mg) were dissolved in 17.5 mL of degassed toluene and heated at 60 °C for 1 h and then 110 °C for 72 h. The reaction mixture was poured into a methanol/HCl (6/1 v/v %) solution. The precipitate was Soxhlet extracted using methanol, hexane, and acetone, dissolved in chloroform, and then reprecipitated from methanol. The precipitated powder was vacuum dried, yielding 875 mg (98%) of material. ^{1}H NMR ($CDCl_3$, 500 MHz) δ (p.p.m.) 8.98 (*b*, 2 H), 7.03 (*b*, 4 H), 4.00 (*b*, 4 H), 1.94 (*b*, 2 H), 1.27–1.21 (*b*, 48 H), 0.85–0.82 (*b*, 12 H) GPC: M_n = 92,000; PDI = 1.6.

For **3**, 3,6-bis(5-bromo-2-thienyl)-2,5-bis(2-hexyldecyl) 2,5-dihydro-pyrrolo[3,4-*c*]pyrrole-1,4-dione (970 mg), 2,2′-bithiophene-5,5′-diboronic acid bis(pinacol) ester (560 mg), K_3PO_4 (1420 mg), and $Pd(dba)_3$ (35 mg) were dissolved in 35 mL of degassed toluene and heated at 60 °C for 1 h and then 90 °C for 72 h. The reaction mixture was purified as described above. Yield 785 mg (65%). ^{1}H NMR ($CDCl_3$, 500 MHz) δ (p.p.m.) 9.24–8.92 (*b*, 4 H), 7.09 (*b*, 4 H), 4.03 (*b*, 4 H), 1.93 (*b*, 2 H), 1.33–1.17 (*b*, 48 H), 0.91–0.76 (*b*, 12 H) GPC: M_n = 9800; PDI = 1.4.

4 was synthesized by the same procedure as was used for **2** using 2,5-bis(trimethylstannyl)thieno[3,2-*b*]thiophene (500 mg). The resulting powder was obtained in 65% yield (610 mg). ^{1}H NMR ($CDCl_3$, 500 MHz) δ (p.p.m.) 9.00 (*b*, 2 H), 6.85 (*b*, 4 H), 3.91 (*b*, 4 H), 2.16 (*b*, 2 H), 1.37–1.08 (*b*, 48 H), 0.92–0.76 (b, 12 H) GPC: M_n = 96,000; PDI = 3.5.

All other reagents were purchased from Sigma-Aldrich Japan and Tokyo Chemical Industry Co., Ltd. and used without further purification. FTO substrates were etched with 1 M HCl and Zn powder (obtained from Nippon Sheet Glass Co.).

Measurements

^{1}H NMR (500 MHz) spectroscopy was conducted with a JEOL ECX500 spectrometer using TMS as a chemical shift standard with $CDCl_3$. Molecular weights were measured by GPC using a TOSOH HLC 8200 instrument with $CHCl_3$ as the eluent and polystyrene standards for calibration. Cyclic voltammetry was performed using an ALS electrochemical analyzer Model 660DX with a platinum disc electrode, an Ag/AgCl electrode calibrated by a ferrocene/ferrocenium redox couple standard, a platinum wire, and 0.1 M $(C_4H_9)_4NClO_4$ chlorobenzene solution as the working, reference, an counter electrode and electrolyte, respectively. X-ray diffraction patterns were obtained with Cu K_α radiation using a Rigaku RINT Ultima III spectrometer. Field-effect mobility was measured with a Keithley 2602 source meter. UV-vis absorption spectra were recorded using a Jasco JW2400 spectrometer. AFM analyses was performed with an MFP3D from Oxford Instruments Co. Gold was evaporated with a VPC-1100 vacuum evaporation system from ULVAC Co. *I-V* characteristics were obtained with a Bunko-keiki CEP-2000MLQ instrument.

Fabrication of the devices

A field-effect transistor was fabricated on a Si substrate. A chlorobenzene solution of each polymer (10 mg/mL) was cast on the substrate and spin-coated at 1000 r.p.m. for 60 s.

Perovskite solar cells were fabricated using a TiO_2 mesoporous substrate. First, a TiO_2 compact layer was formed on the FTO substrate via spray-pyrolysis with a titanium acetylacetonate/ethanol solution (1/4 v/v) at 320 °C. A TiO_2 dispersion (PST-18NR, Nikki Shokubai Kasei Co.) was spin-coated at 4000 r.p.m. for 30 s to achieve a thickness of ~200 nm, and after soaking in aqueous $TiCl_4$ solution, the substrate was heated at 70 °C for 1 h and sintered at 500 °C for 30 min. A perovskite precursor solution was prepared by dissolving lead iodide (1.84 g) and methylammonium iodide (636 mg) in a mixture of DMSO (0.28 mL) and DMF (2.54 mL) for 1 h at room temperature, and then the solution was spin-coated on the mesoporous TiO_2 layer at 4000 r.p.m. for 30 s. The formamidinium- and Cs-containing perovskite was prepared by dissolving formamidine hydroiodide (516 mg), methylamine hydrobromide (67.2 mg), lead iodide (1.52 g), lead bromide (223 mg), and cesium iodide (48.9 mg) powders in a mixture of DMF (2.4 mL), DMSO (0.74 mL), and acetonitrile (0.12 mL) [39, 40]. The Rb-containing perovskite layer was prepared by dissolving formamidine hydroiodide (516 mg), methylamine hydrobromide (67.2 mg), lead iodide (1.52 g), lead bromide (242 mg), cesium iodide (48.9 mg), and rubidium iodide (40.2 mg) powders in a mixture of DMF (2.4 mL), DMSO (0.34 mL), and acetonitrile (0.26 mL) [41]. Chlorobenzene (500 µL) was dropped onto the substrate during the spin-coating procedure. After annealing at 65 °C for 1 min and at 100 °C for 2 min, the chlorobenzene solution of the polymer (7.5 mg/mL) was spin-coated to form the hole-transporting layer. All spin-coating processes were conducted in a glove box. Au was deposited on the polymer layer under vacuum (2.0×10^{-4} Pa) at a rate of 0.1 nm/s to form a Au layer with a thickness of ~50 nm.

Results and discussion

Diketopyrrolopyrrole (DPP) thiophene polymers **1**–**4** were synthesized via one-step coupling reactions of the 3,6-bis-bromo derivative, 3,6-bis(5-bromo-2-thienyl)-2,5-bis(2-hexyldecyl)-2,5-dihydro-pyrrolo[3,4-*c*]pyrrole-1,4-dione, as the DPP source via Yamamoto, Stille, and Suzuki coupling reactions for **1**, **2** and **4**, and **3**, respectively (Scheme 1), by modifying reaction conditions previously reported in the literature [37, 38]. Despite the strong π–π interpolymer interactions, the polymers with molecular weights of 10^4–10^5 were soluble in common organic solvents such as chloroform, chlorobenzene, and tetrahydrofuran (except **1** in THF), which was attributed to their branched alkyl side chains.

Cyclic voltammograms of the polymers in the chlorobenzene solution displayed reversible redox waves in the range of 0.5–0.9 V, which were attributed to a redox or doping reaction of the thiophene moieties of the polymers (see Supplementary Information Figure S1). **4** gave two redox peaks due to the redox potential difference of the thiophene and the thienothiophene moieties. The HOMO energy levels were estimated from the redox potentials determined from cyclic voltammetry and are given in Table 1, and these data are comparable to those reported in previous papers [26–31].

The polymers showed weak absorption at 800–950 nm (Supplementary Figure S2). Nearly planar structures were estimated based on Gaussian calculations of the DPP units in the dimer analogues of polymers **1**–**4** polymers (Supplementary Figure S3), which suggested a planar, π-conjugated polymer backbone due to effective sp^2 orbital overlap.

X-ray diffraction of the DPP polymers measured with parallel X-ray beams exhibited a profile with two sharp peaks (Supplementary Figure S4), which indicates that the polymers are semicrystalline. The low angle peak was attributed to a lamellar structure and gave the lattice spacing, and the high angle peak at 23° gave a π–π stacking distance of 3.6–3.8 Å (Table 1, 4Å for similar polymers in a previous paper [27]). The smaller π–π stacking distance and lattice spacing for polymer **4** compared to those of **1**–**3**

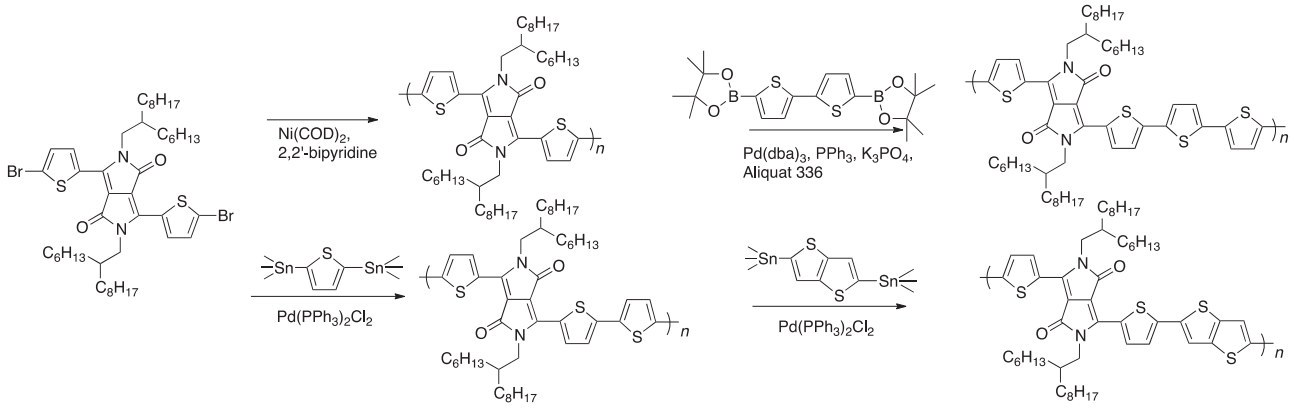

Scheme 1 Preparation of the diketopyrrolopyrrole-thiophene polymers

Table 1 Energy levels, structural parameters, and hole mobilities of the DPP polymers

Polymer	HOMO[a] (-eV)	LUMO[b] (-eV)	E_g[c] (eV)	Dihedral angle (deg)	Hole mobility (10^{-2} cm^2/Vs)	Lattice spacing[d] (Å)	π–π stacking distance[d] (Å)
1	5.34	3.99	1.35	179.99	0.0088	20	3.8
2	5.20	3.62	1.58	179.92	4.4	19	3.8
3	5.25	3.85	1.40	179.91	0.0027	19	3.8
4	5.19	3.64	1.54	179.85	3.7	17	3.6

[a]HOMO (eV) = $E_{Ag/AgCl} + 4.66$ (Supplementary Figure S1)

[b]Calucurated by using the *HOMO* level and E_g

[c]Band gaps (E_g) of the polymers were estimated with absorption edges of UV-vis spectra (Supplementary Figure S2)

[d]Calculated by XRD (Supplementary Figure S4)

suggested a closely packed and semicrystalline polymer structure.

The hole mobility of the polymers was estimated from the linear current region (Figure S5) of the field-effect transistors fabricated with **1**–**4**, and the values are listed in Table 1. The transistors displayed on/off switching behavior. The mobilities were calculated with the equation $\mu = L/WC_iV_{DS}(\delta I_D/\delta V_G)$, where L and W are the semiconductor channel length and width, respectively, C_i is the capacitance per unit area of the gate dielectric layer, V_{DS} and δV_G are the drain-source voltage and changed portion of gate voltage, respectively, and δI_D is the changed portion of drain current. Polymers **2** and **4** showed higher hole mobilities (on the order of 10^{-2} cm^2/Vs) than those of **1** and **3**, which was consistent with their smaller d spacing and higher molecular weights.

AFM images of the spin-coated layers suggested very smooth layer formation with small roughnesses of <10 nm, which is suitable for a hole-transporting layer of a device (Supplementary Figure S6).

The DPP polymers were used as the hole-transporting layer of perovskite-type solar cells. The excellent film-forming properties of the polymers resulted in a uniform, 50-nm thick layer on the perovskite layer (Fig. 1). The formation of such a thin and defect-free layer is a crucial advantage of hole-transporting polymers in comparison with low-molecular-weight materials.

The cells were subjected to current density–voltage (J–V) measurements under 1 sun irradiation (Fig. 2 and Table 2). The cells prepared with polymers **2** and **4**, which have higher hole mobilities, displayed smaller series resistance than those of the cells with **1** and **3** and yielded larger fill factors (*FF* values, Table 2). We further optimized the fabrication of the perovskite layer by adding formamidinium, Cs, and Rb as cations (see the "experimental" section) [39–41]. The optimized Rb-containing perovskite layer increased the conversion efficiency to 16.3% without any additives, such as an oxidizing dopant, a salt such as lithium bis(trifluoromethanesulfonyl)imide (LiTFSI), or a base such as *tert*-butyl pyridine (for the reproducibility data, see Supplementary Figure S7). A conversion efficiency greater than 16% would be among the best performances of dopant-free polymer-based solar cells reported to date [28, 29]. The high carrier mobility of the DPP polymer and the thin-film formability could contribute to the hole transport function of the layer, and the electron-donating capability of the thiophene moiety may assist in extracting holes at the perovskite interface.

The photoconversion efficiency of ~16% was maintained for almost one month when the cells were kept in a dry,

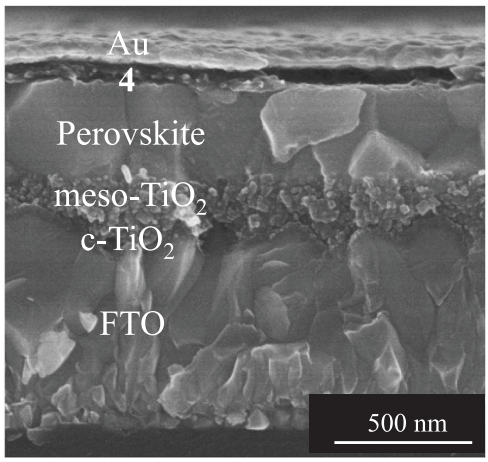

Fig. 1 Cross-sectional SEM image of the perovskite solar cell fabricated with **4** as the hole transporting material

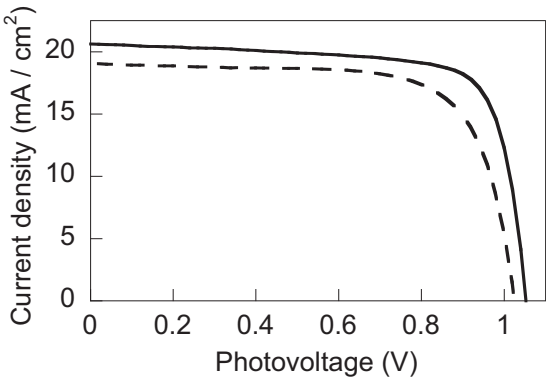

Fig. 2 *J–V* characteristics of the perovskite solar cells fabricated with the (——)RbCsMAFAPb$(BrI)_3$ perovskite and the (--)Cs MAFAPb $(BrI)_3$ perovskite and **4** as the hole-transporting material. MA methylammonium, FA formamidinium

Table 2 Current density (J_{sc}), open-circuit potential (V_{oc}), fill factor (*FF*), and photovoltaic performance (η) of the perovskite solar cells fabricated with the DPP polymers as the hole transporting material

HTM	J_{sc} (mA/cm^2)	V_{oc} (V)	*FF* (-)	η (%)
1	13.9	0.94	0.54	7.1
2	11.5	0.94	0.67	7.3
3	9.1	0.90	0.55	4.5
4	13.1	0.95	0.74	9.1
$\mathbf{4_{Cs}}$	19.7	1.01	0.72	14.2
$\mathbf{4_{Rb}}$	20.6	1.05	0.75	16.3

dark place at room temperature. It has been reported that dopants often absorb moisture and/or migrate into the perovskite and titanium oxide layers to degrade the cell performance (Supplementary Figure S8). The hole-transport layer composed of the dopant-free and genuine DPP polymers was credited with the durability of the highly efficient perovskite solar cell.

Acknowledgements This work was partially supported by "Research and Development of Innovative Nano Structure Solar Cells" from NEDO, Japan. HM and KS acknowledge the Leading Graduate Program in Science and Engineering, Waseda University from MEXT, Japan.

Compliance with ethical standards

Conflict of interest The authors declare that they have no conflict of interest.

References

1. Guo X, Baumgarten M, Müllen K. Designing π-conjugated polymers for organic electronics. Prog Polym Sci. 2013;38:1832–908.
2. Rivnay J, Mannsfeld SCB, Miller CE, Salleo A, Toney MF. Quantitative determination of organic semiconductor microstructure from the molecular to device scale. Chem Rev. 2012;112:5488–519.
3. Jikei M, Mori R, Kawauchi S, Kakimoto M, Taniguchi Y. Synthesis and properties of hyperbranched poly(triphenylamine)s prepared by palladium catalyzed C–N coupling reaction. Polym J. 2002;34:550–7.
4. Davis AR, Maegerlein JA, Carter KR. Electroluminescent networks via photo "click" chemistry. J Am Chem Soc. 2011;133:20546–51.
5. Michinobu T. Click functionalization of aromatic polymers for organic electronic device applications. Macromol Chem Phys. 2015;216:1387–95.
6. Saito M, Osaka I. Impact of side chain placement on thermal stability of solar cells in thiophene–thiazolothiazole polymers. J Mater Chem C. 2018. https://doi.org/10.1039/C7TC04721E.
7. Fukuta S, Higashihara T. Ternalization approach for tuning light absorption and crystalline structure of diketopyrrolopyrrole-based polymer using bisthiadiazole unit. J Electrochem Soc. 2018;165:B3001–5.
8. Zhou E, Yamakawa S, Tajima K, Yang C, Hashimoto K. Synthesis and photovoltaic properties of diketopyrrolopyrrole-based donor−acceptor copolymers. Chem Mater. 2009;21:4055–61.
9. Kaur M, Choi DH. Diketopyrrolopyrrole: brilliant red pigment dye-based fluorescent probes and their applications. Chem Soc Rev. 2015;44:58–77.
10. Liu F, Wang C, Baral JK, Zhang L, Watkins JJ, Briseno AL, et al. Relating chemical structure to device performance via morphology control in diketopyrrolopyrrole-based low band gap polymers. J Am Chem Soc. 2013;135:19248–59.
11. Yang L, Yu Y, Gong Y, Li J, Ge F, Jiang L, et al. Systematic investigation of the synthesis and light-absorption broadening of a novel diketopyrrolopyrrole conjugated polymer of low and high molecular weight with thermo-labile groups. Polym Chem. 2015;6:7005–14.
12. Kuwabara J, Takase N, Yasuda T, Kanbara T. Synthesis of conjugated polymers possessing diketopyrrolopyrrole units bearing phenyl, pyridyl, and thiazolyl groups by direct arylation polycondensation: effects of aromatic groups in DPP on physical properties. J Polym Sci Part A Polym Chem. 2016;54:2337–45.
13. Kuwabara J, Yamagata T, Kanbara T. Solid-state structure and optical properties of highly fluorescent diketopyrrolopyrrole derivatives synthesized by cross-coupling reaction. Tetrahedron Lett. 2010;66:3736–41.
14. Cho M, Shin J, Hong T, Um H, Lee TW, Kim G, et al. Diketopyrrolopyrrole-based copolymers bearing highly

π-extended donating units and their thin- film transistors and photovoltaic cells. Polym Chem. 2015;6:150–9.
15. Cho M, Shin J, Yoon SH, Lee TW, Kaur M, Choi DH. A high-mobility terselenophene and diketopyrrolopyrrole containing copolymer in solution-processed thin film transistors. Chem Commun. 2013;49:7132–4.
16. Bronstein H, Chen Z, Ashraf RS, Zhang W, Du J, Durrant JR, et al. Thieno[3,2-*b*]thiophene-diketopyrrolopyrrole-containing polymers for high-performance organic field-effect transistors and organic photovoltaic devices. J Am Chem Soc. 2011;133:3272–5.
17. Yao J, Yu C, Liu Z, Luo H, Yang Y, Zhang G, et al. Significant improvement of semiconducting performance of the diketopyrrolopyrrole–quaterthiophene conjugated polymer through side-chain engineering via hydrogen-bonding. J Am Chem Soc. 2016;138:173–85.
18. Kim G, Kang S, Dutta GK, Han Y, Shin TJ, Noh Y, et al. Thienoisoindigo-naphthalene polymer with ultrahigh mobility of 14.4 $cm^2/V{\cdot}s$ that substantially exceeds benchmark values for amorphous silicon semiconductors. J Am Chem Soc. 2014;136:9477–83.
19. Lee JS, Son SK, Song S, Kim H, Lee DR, Kim K, et al. Importance of solubilizing group and backbone planarity in low band gap polymers for high performance ambipolar field-effect transistors. Chem Mater. 2012;24:1316–23.
20. Ha JS, Kim KH, Choi DH. 2,5-Bis(2-octyldodecyl)pyrrolo[3,4-*c*]pyrrole-1,4-(2*H*,5*H*)-dione-based donor–acceptor alternating copolymer bearing 5,5′-di(thiophen-2-yl)-2,2′-biselenophene exhibiting 1.5 $cm^2{\cdot}V^{-1}{\cdot}s^{-1}$ hole mobility in thin-film transistors. J Am Chem Soc. 2011;133:10364–7.
21. Li Y, Sonar P, Singh SP, Soh MS, Meurs M, Tan J. Annealing-free high-mobility diketopyrrolopyrrole-quaterthiophene copolymer for solution-processed organic thin film transistors. J Am Chem Soc. 2011;133:2198–204.
22. Li Y, Sun B, Sonar P, Singh SP. Solution processable poly(2,5-dialkyl-2,5-dihydro-3,6-di-2-thienyl- pyrrolo[3,4-c]pyrrole-1,4-dione) for ambipolar organic thin film transistors. Org Electron. 2012;13:1606–13.
23. Dou L, Gao J, Richard E, You j, Chen C, Cha KC, et al. Systematic investigation of benzodithiophene- and diketopyrrolopyrrole-based low-bandgap polymers designed for single junction and tandem polymer solar cells. J Am Chem Soc. 2012;134:10071–9.
24. Walker B, Tamayo AB, Dang X, Zalar P, Seo H, Garcia A, et al. Nanoscale phase separation and high photovoltaic efficiency in solution-processed, small-molecule bulk heterojunction solar cells. Adv Funct Mater. 2009;19:3063–9.
25. Choi M, Ko EJ, Han YW, Lee EJ, Moon DK. Control of polymer-packing orientation in thin films through chemical structure of D-A type polymers and its application in efficient photovoltaic devices. Polym (Guildf). 2005;74:205–15.
26. Suwa K, Tanaka S, Oyaizu K, Nishide H. Arylamine polymers prepared via facile paraldehyde-addition condensation: an effective hole-transporting material for perovskite solar Cells. Polym Int. 2018;67:670–4.
27. Zhang F, Wang Z, Zhu H, Pellet N, Luo J, Yi C, et al. Over 20% PCE perovskite solar cells with superior stability achieved by novel and low-cost hole-transporting materials. Nano Energy. 2017;41:469–75.
28. Kinoshita T, Nonomura K, Jeon NJ, Giordano F, Abate A, Uchida S, et al. Spectral splitting photovoltaics using perovskite and wideband dye-sensitized solar cells. Nat Commun. 2015;6:8834–41.
29. Ahn N, Son D, Jang I, Kang S, Choi M, Park N. Highly reproducible perovskite solar cells with average efficiency of 18.3% and best efficiency of 19.7% fabricated via lewis base adduct of lead(II) iodide. J Am Chem Soc. 2015;137:8696–9.
30. Kojima A, Teshima K, Shirai Y, Miyasaka T. Organometal halide perovskites as visible-light sensitizers for photovoltaic cells. J Am Chem Soc. 2009;131:6050–1.
31. Cojocaru L, Uchida S, Sanehira Y, Nakazaki J, Kubo T, Segawa H. Surface treatment of the compact TiO_2 layer for efficient planar heterojunction perovskite solar cells. Chem Lett. 2015;44:674–6.
32. Zhao Y, Tan H, Yuan H, Yang H, Fan JZ, Kim J, et al. Perovskite seeding growth of formamidinium-lead- iodide-based perovskites for efficient and stable solar cells. Nat Commun. https://doi.org/10.1038/s41467-018-04029-7.
33. Yang WS, Noh JH, Jeon NJ, Kim YC, Ryu S, Seo J, et al. High-performance photovoltaic perovskite layers fabricated through intramolecular exchange. Science. 2015;348:1234–7.
34. Yang WS, Park BW, Jung EH, Jeon NJ, Kim YC, Lee DU, et al. Iodide management in formamidinium-lead-halide–based perovskite layers for efficient solar cells. Science. 2017;356:1376–9.
35. Ameen S, Rub MA, Kosa SA, Alamry KA, Akhtar MS, Shin HS, et al. Perovskite solar cells: influence of hole transporting materials on power conversion efficiency. ChemSusChem. 2016;9:10–27.
36. Heo JH, Han HJ, Kim D, Ahn TK, Im SH. Hysteresis-less inverted $CH_3NH_3PbI_3$ planar perovskite hybrid solar cells with 18.1% power conversion efficiency. Energy Environ Sci. 2015;8:1602–8.
37. Kwon YS, Lim J, Yun HJ, Kim YH, Park T. A diketopyrrolopyrrole-containing hole transporting conjugated polymer for use in efficient stable organic–inorganic hybrid solar cells based on a perovskite. Energy Environ Sci. 2014;7:1454–60.
38. Dubey A, Adhikari N, Venkatesan S, Gu S, Khatiwada D, Wang Q, et al. Solution processed pristine PDPP3T polymer as hole transport layer for efficient perovskite solar cells with slower degradation. Sol Energy Mater Sol Cells. 2016;145:193–9.
39. Zhang Y, Grancini G, Feng Y, Asiri AM, Nazeeruddin MK. Optimization of stable quasi-cubic FAxMA1−xPbI3 perovskite structure for solar cells with efficiency beyond 20%. ACS Energy Lett. 2017;2:802–6.
40. Saliba M, Matsui T, Seo JY, Domanski K, Correa-Baena JP, Nazeeruddin MK, et al. Cesium-containing triple cation perovskite solar cells: improved stability, reproducibility and high efficiency. Energy Environ Sci. 2016;9:1989–97.
41. Saliba M, Matsui T, Domanski K, Seo JY, Ummadisingu A, Zakeeruddin SM, et al. Incorporation of rubidium cations into perovskite solar cells improves photovoltaic performance. Science. 2016;354:206–9.